Available online at www.sciencedirect.com

ScienceDirect

journal homepage: www.elsevier.com/locate/he

Optimization of the operating conditions for steam reforming of slow pyrolysis oil over an activated biochar-supported Ni–Co catalyst

Christian Di Stasi [a,*], *Marta Cortese* [b], *Gianluca Greco* [a], *Simona Renda* [b], *Belén González* [a], *Vincenzo Palma* [b], *Joan J. Manyà* [a]

[a] *Aragón Institute of Engineering Research (I3A), Thermochemical Processes Group, University of Zaragoza, Escuela Politécnica Superior, Crta. Cuarte s/n, 22071, Huesca, Spain*

[b] *University of Salerno, Department of Industrial Engineering, Via Giovanni Paolo II 132, 84084, Fisciano (SA), Italy*

HIGHLIGHTS

- Activated biochar is a suitable catalyst support for the upgrading of pyrolysis oil.
- Ni–Co catalyst showed the best performance in acetic acid steam reforming.
- Heavy organic compounds could poison the metallic active sites of the catalyst.
- Steam reforming of pyrolysis oil was achieved with a carbon conversion of 65%.
- No catalyst deactivation was observed during the first 850 min.

GRAPHICAL ABSTRACT

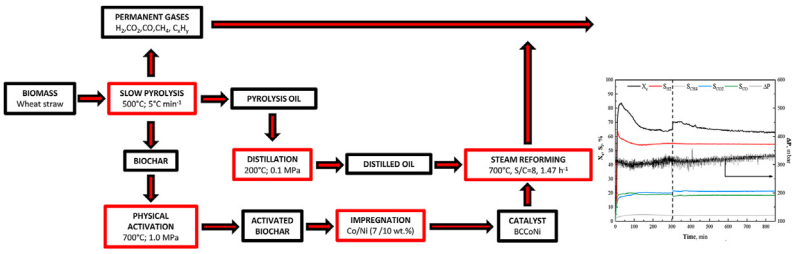

ARTICLE INFO

Article history:
Received 10 March 2021
Received in revised form
20 May 2021
Accepted 26 May 2021
Available online 17 June 2021

Keywords:
Bio-oil
Steam reforming
Pyrolysis

ABSTRACT

Highly performing activated biochar-based catalysts were produced for steam reforming of slow pyrolysis oil. The raw biochar obtained from the slow pyrolysis step was physically activated with CO_2 at 700 °C and 1.0 MPa and then employed as support. Preliminary tests on steam reforming of acetic acid at 600 °C showed that using activated biochar-supported catalysts containing 10 wt % Ni and 7 wt % Co led to a conversion above 90% with a relatively slow deactivation rate. When a representative organic model compounds mixture was used as feed, relatively fast deactivation of the catalyst was observed, probably due to the adsorption of heavy organic compounds, which could subsequently react to form not easily desorbable reaction intermediates. However, the dual Ni–Co catalysts exhibited a good performance during the steam reforming of a real slow pyrolysis oil at 750 °C, showing long stability and a constant carbon conversion of 65%.

* *Corresponding author.*
E-mail address: christiandistasi@unizar.es (C. Di Stasi).

https://doi.org/10.1016/j.ijhydene.2021.05.193

Catalyst
Model compound

Introduction

Pyrolysis oil is a side-product obtained from the pyrolysis or gasification of biomass. Despite its composition strictly depends on biomass nature and pyrolysis conditions, it is usually composed of a high fraction of water (especially for slow pyrolysis processes) and a complex mixture of oxygenated organic compounds (produced from the decomposition of the main biomass constituents) [1–3]. The high contents of water and the heterogeneity of its composition make slow pyrolysis-derived bio-oil not appropriate to be used as fuel [4]. Moreover, the main problem is that it could condensate in the reactor or pipes, causing plant breakdowns. Thus, upgrading pyrolysis vapors via steam reforming represents an interesting option to avoid the above-mentioned problems [5–7].

A very detailed list of all the reactions involved in bio-oil upgrading could be found in the work by Hu et al. [8]. The syngas generated by the pyrolysis oil steam reforming could be supplied to processes such as Fischer-Tropsch, hydrotreating, and ammonia or methanol synthesis [9]. Given that the main steam reforming reaction is endothermic, the pyrolysis outlet stream could be directly fed to the reformer without the need to cool down the gaseous stream. Furthermore, the high water content present in the pyrolysis oil could be sufficient to obtain a relatively high yield of hydrogen without the need to add water from external sources. However, in order to increase the reactants conversion and the desired products yield, the employment of a catalyst is mandatory. The production of highly efficient and selective catalysts requires the use of Rh, Pt, or Ir, which is discouraged due to their excessive cost [10]. A good trade-off between cost and efficiency is given by the employment of transition metals, mainly Ni [11], Fe [12], Co [13], alkaline metals such as K [7], and rare earth metals as Ce [14], which are widely used in catalytic formulations for steam reforming.

The most significant challenge in reforming processes, in particular when heavy compounds are involved as hydrocarbon source, is to achieve a good catalyst stability, which is quite difficult considering all the possible deactivation phenomena, mainly related to metal sintering or coke deposition, being the latter the most relevant pathway for catalyst deactivation [15–17]. Secondary and undesired reactions, which lead to the formation of undesired by-products, can be hindered through a reasonable choice of the support. Alumina, olivine, mixed Ce and Zn oxides, HZSM-5, and carbon nanotubes are the most used supports for steam reforming catalysts [18]. The main drawback, however, is the relatively high cost of these supports, since their synthesis involves energy-intense processes [12]. As an alternative, biochar-based catalysts are gaining interest year after year due to their relatively low price, easy functionalization, and versatility [19–21]. Furthermore, at their end-life stage, they could be gasified/burned to recover energy and active phases [22,23]. Biochar is generally produced by biomass slow pyrolysis, which guarantees relevant solid yield [24]. The resulting pristine biochar is usually characterized by poor textural properties (i.e., very low surface area and porosity) [25,26]. Relatively large surface areas and tailor-made pore size distributions are usually key features for catalyst supports. Fortunately, the porosity of pristine biochar can easily be engineered through activation post-treatments, leading to refined carbon materials with high potential to ensure a homogeneous loading of a given active phase [27,28]. In the last years, a growing number of research studies focused on using biochar-based catalysts for pyrolysis oil upgrading purposes [29–32]. However, catalytic steam reforming of a model compound, instead of real pyrolysis oil, is usually reported in the majority of previous works.

The specific aim of this work was to perform a comprehensive study on the suitability of activated biochar-derived catalysts to be used in the steam reforming of slow pyrolysis oil. For this purpose, several mono and bimetallic catalysts were produced using Ni, Co, K, Ce, and Fe as active phases. Due to the complex composition of the pyrolysis oil, model compounds were firstly used to test the performances of produced catalysts. Firstly, steam reforming of acetic acid was carried out to identify the best catalytic formulation. Then, a more complex model mixture (composed of acetone, acetic acid, eugenol, and ethanol) was employed to optimize the operating conditions and to study the deactivation mechanism. In the final experimental stage, steam reforming of a real pyrolysis oil was tested.

Experimental section

Catalysts production

The biochar used in this study was produced by slow pyrolysis (at 500 °C and 0.1 MPa) of binder-free wheat straw pellets (9 mm OD and 10–13 mm long). The pristine biochar was then physically activated with pure CO_2 at 700 °C and 1.00 MPa in order to increase its specific surface area and pore size distribution (PSD). The choice of the activation conditions was based on the results of a previous work, in which the beneficial effect of pressure on the mesoporosity development of the resulting activated biochars was observed. More details on the pyrolysis and activation procedure are available elsewhere [28,33,34].

The metallic active phases were deposited on the carbonaceous support via wet impregnation. $Fe(NO_3)_3 \cdot 9H_2O$, $Ni(NO_3)_2 \cdot 6H_2O$, $Co(NO_3)_2 \cdot 6H_2O$, $Ce(NO_3)_3 \cdot 6H_2O$ and KNO_3 were used as precursors of the catalyst active phase. The percentage of the

metal loading was relative to the mass of activated biochar used as support. Briefly, the activated biochar was impregnated with an aqueous solution of the precursor salt containing the desired loading of the active phase and then stirred at 60 °C until complete water evaporation. The impregnated sample was then dried overnight at 110 °C. After that, the catalysts were calcinated for 3 h at 600 °C under N_2 flow to decompose all the precursor salts and subsequently sieved in order to obtain a particle size distribution in the range of 0.125–0.250 mm. The bimetallic catalysts were prepared in four steps: (1) deposition of the first precursor; (2) calcination; (3) impregnation of the second precursor; and (4) final calcination. The employed nomenclature and a resume of the produced catalysts are reported in Table 1.

Table 1 – Resume of the mono and bimetallic catalysts prepared and tested in this work.

Support	Sample	Active phase	Loading (wt. %)
	BC	/	/
Monometallic			
	BCFe	Fe	7
	BCCo	Co	7
	BCCe	Ce	7
	BCK	K	7
	BCNi7	Ni	7
	BCNi4	Ni	4
	BCNi10	Ni	10
Bimetallic			
	BCFeNi	Fe/Ni	7/10
	BCCoNi	Co/Ni	7/10
	BCCeNi	Ce/Ni	7/10
	BCKNi	K/Ni	7/10

Characterization of carbon materials and liquids

The textural properties of the activated biochar support (BC) and calcinated catalysts were determined from the N_2 adsorption/desorption isotherms at −196 °C, which were obtained using an ASAP 2020 automatic adsorption analyzer (Micromeritics, USA). Around 120 mg of sample was degassed under vacuum at 150 °C. The specific surface area was evaluated using the Langmuir model (S_L); total pore volume (V_{tot}) was obtained from the N_2 adsorbed at high relative pressure (0.99); the specific volume of micropores (V_{micro}) was calculated using the t-plot method; the mesopore volume (V_{meso}) was evaluated from the pore size distribution (assuming a non-local density functional theory, NLDFT, and slit-pore geometry) by subtracting the cumulative volume of the smaller pores (d_p < 2 nm) from the total volume (d_p < 50 nm). The software MicroActive from Micromeritics was used for all the above-mentioned calculations.

The activated biochar support was also characterized by proximate analysis (in quadruplicate according to ASTM standards) and ultimate analysis (CHN), which was carried out using an elemental analyzer model CHN628 from Leco Corporation (USA). X-Ray Fluorescence (XRF) spectroscopy analysis (using an ADVANT'XP + XRF spectrometer from Thermo ARL, Switzerland) was also carried out to identify and quantify the inorganic species available in the biochar ash.

The moisture content of the pyrolysis oil was evaluated by Karl-Fischer titration. Ultimate analysis, including the sulfur content, was also performed for pyrolysis oil using the same elemental analyzer described above.

The reducibility properties of the prepared biochar-based catalysts were investigated by means of temperature-programmed reduction (TPR) analysis. To this aim, 0.5 g of each sample was loaded into the reactor and heated under a reducing stream (5% H_2 in Ar, at a flow rate of 0.5 NL min^{-1}) at a heating rate of 15 °C min^{-1} from 50 to 600 °C. The hydrogen concentration at the outlet was continuously monitored by means of a Hiden QGA mass spectrometer (Hiden Analytical, UK).

CO_2 temperature-programmed desorption (CO_2-TPD) was also used to investigate the surface properties of the prepared catalysts. It is generally recognized that CO_2-TPD allows the determination of weak, medium, and strong basic sites on the catalyst surface [35,36]. The analysis was conducted as follows: CO_2 adsorption was firstly performed at 50 °C on 0.5 g of the reduced catalyst under a stream of CO_2 in Ar (40 vol % CO_2) for 30 min; then, weakly adsorbed CO_2 was purged with a pure Ar stream at the same temperature for 1 h; finally, CO_2-TPD was performed in pure Ar raising the temperature from 50 to 700 °C at a heating rate of 5 °C min^{-1}. Desorbed CO_2 was measured by means of the above-mentioned mass spectrometer.

In order to observe the morphology of the coke deposition and the dimension of the metallic nanoparticles, transmission electron microscopy (TEM) of fresh and spent catalysts was carried out using a Tecnai F30 microscope (FEI, USA) operating at 300 kV. Samples were previously sonicated for 5 min in an aqueous solution of ethanol.

Catalytic tests

Catalytic tests were carried out in a tubular fixed-bed reactor (made of Hastelloy C276, 300 mm long and 10 mm ID) placed in an electric tubular furnace. Around 0.5 g of sample was located inside the reactor and packed with an inert filler (Kaowool™ fiber). A K-type thermocouple placed in the middle of the catalytic bed was used to monitor the system temperature. Prior to each steam reforming experiment, the catalyst was heated up to 600 °C under reducing atmosphere (N_2/H_2, 50/50 vol %). These conditions were kept for 2.5 h to assure complete reduction of the active metal oxides.

Since the pyrolysis oil is a very complex mixture of hundreds of organic compounds, the study was firstly carried out using representative model compounds. In a first stage, an aqueous solution of acetic acid (steam to carbon molar ratio, S/C, of 4) was used to study the performance of the different catalysts. The reason behind this choice lays in the high content of this carboxylic acid in slow pyrolysis oils (up to 20 wt %) [37–39] and in the availability of numerous studies in the literature, which can be useful for comparison purposes. In a second stage, an equimass mixture of acetone, acetic acid, ethanol, and eugenol was used for the best performing catalyst during acetic acid reforming. These compounds were

chosen as representative products from the thermal decomposition of lignin, cellulose, and hemicelluloses [37,40,41]. Finally, steam reforming of real pyrolysis oil was carried out using the liquid collected during the production of the pristine biochar.

Steam reforming experiments were carried out at different temperatures in the range of 400–750 °C. The liquid blend was fed using a HPLC pump, maintaining a liquid hourly space velocity (LHSV) of the organic fraction equal to 2.94 h^{-1} (considering a bed void fraction of 0.5). The liquid was forced to pass through a coil wrapped around a cartridge resistance, to reach complete evaporation of the blend, and mixed with N_2 to be delivered to the reactor. The composition of the outlet gas was monitored using the above-mentioned spectrometer, which was able to measure, in real-time, the concentrations of acetic acid, acetone, and permanent gases. For steam reforming of the model mixture and real pyrolysis oil, the gas composition was analyzed using a dual-channel micro-gas chromatograph (μ-GC 490 from Agilent, USA) equipped with TCD detectors and two analytical columns (a Molsieve 5 A and a PoraPlot U). The known amount of N_2 fed was used as tracking compound to calculate the mass of produced gas. The evolution of the pressure drop along the reactor was measured employing a differential pressure sensor. A schematic overview of the experimental device is given in Fig. 1.

The performance of the different catalysts tested was evaluated in terms of acetic acid conversion (X_{AcOH}), as well as hydrogen (Y_{H2*}), and acetone yield (Y_{Ac*}), as defined in Eq. (1)–(3). On the other hand, for the results obtained using the model mixture and real pyrolysis oil, the carbon conversion (X_C), product yield (Y_i), and selectivity (S_i) were calculated according to Eq. (4)–(6). In such equations, F_i is the molar flow rate of the "i" specie; F_c is the carbon molar flow rate (which was calculated considering all the species detected by the μ-GC: CO, CO_2, and CH_4); and F_{iEq} is the molar flow rate of the "i" specie at the thermodynamic equilibrium condition (which was calculated using the process simulation software Aspen Plus v. 10 from Gibbs free energies).

$$X_{AcOH} = \frac{F_{AcOH,in} - F_{AcOH,out}}{F_{AcOH,in}} 100 \quad (1)$$

$$Y_{H2*} = \frac{1}{4}\frac{F_{H2,out}}{F_{AcOH,in}} 100 \quad (2)$$

$$Y_{Ac*} = 2\frac{F_{Ac,out}}{F_{AcOH,in}} 100 \quad (3)$$

$$X_C = \frac{F_{C,out}}{F_{C,in}} 100 \quad (4)$$

$$Y_i = \frac{F_{i,out}}{F_{iEq,\ out}} 100 \quad (5)$$

$$S_i = \frac{F_{i,out}}{F_{H2,\ out} + F_{CO2,\ out} + F_{CO,\ out} + F_{CH4,\ out}} 100 \quad (6)$$

Results and discussion

Catalysts characterization

Results from proximate, ultimate, and inorganic matter analyses of the activated carbon (BC), which was used as support, are reported in Table 2. The most important textural properties for all the produced catalysts are shown in Fig. 2. The high ash percentage of BC was the result of the activation procedure, which created a high specific surface area through the gasification of the carbon structure, leading to an increase in the specific ash content. The inherent inorganic matter of biomass could promote the gasification of the coke produced during the course of the reforming experiments [12,26,42,43]. As shown in Fig. 2, the activated carbon (BC) had the highest

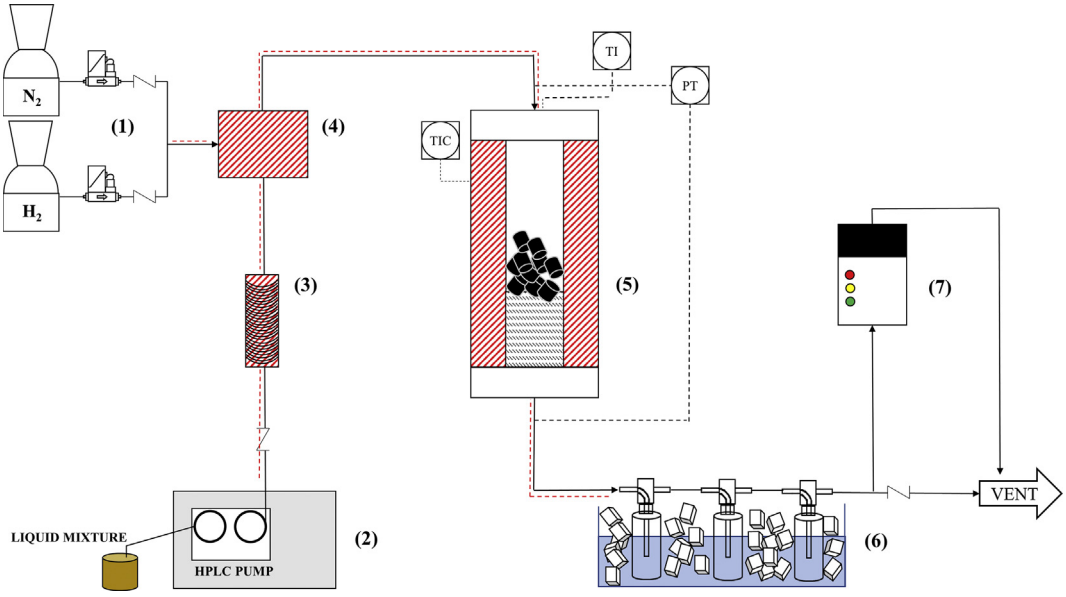

Fig. 1 – Schematic overview of the experimental device used in this work: feeding system (1); HPLC pump (2); evaporator (3); gas mixer (4); fixed-bed reactor and furnace (5); condensation train (6); and μ-GC analyzer/quadrupole mass spectrometer (7).

Table 2 – Proximate, ultimate, and inorganic matter (as oxides) analyses of the physically activated biochar employed as support of the produced catalysts.

Ultimate analysis (wt.%)	
Carbon	61.59
Hydrogen	1.16
Nitrogen	1.84
Oxygen[a]	35.40
Proximate analysis (wt.%)	
Moisture	N.D.
Volatiles	8.16
Ashes	41.98
Fixed Carbon[a]	50.75
Inorganic matter (wt.%)	
SiO_2	17.52
K_2O	16.68
CaO	7.40
P_2O_5	2.45
MgO	1.51
Al_2O_3	1.11
Fe_2O_3	1.05
S	0.716
Cl	0.702
Na_2O	0.216

[a] Values calculated by difference.

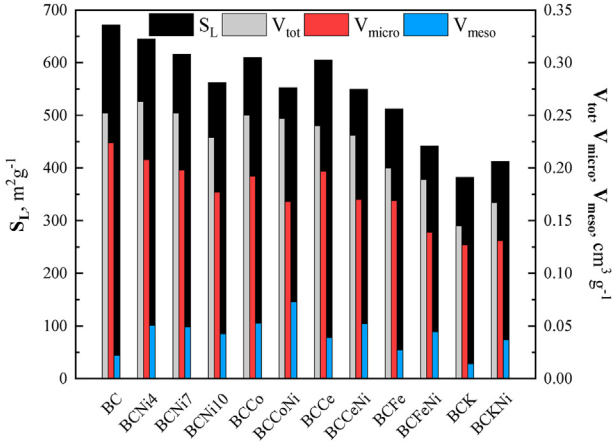

Fig. 2 – Specific surface area (Langmuir, S_L) and pore volumes (V_{tot}, V_{micro}, and V_{meso}) of the twelve catalysts produced in the present study.

specific surface area, which was mainly contributed by micropores. In general, the impregnation and subsequent calcination steps of the resulting BC-based catalysts led to a decrease in the surface area (see Fig. 2). The magnitude of this observed reduction depends on the nature and loading of the active metal phase, which could partly clog the pores of the support, leading to a decrease in the available surface area. Furthermore, an increase in the volume of mesopores at the expense of that of micropores was observed for BC-based catalysts. This could be attributed to interactions between the carbon matrix, which has reductive properties [31,44], and the metal oxides resulting from the decomposition of the precursor salts [45–47]. Recently, Li et al. [48] have reported an increase in the mesopore volume of Ni-laden chemically activated biochars. The authors ascribed this increase in mesoporosity to the role of Ni in promoting the decomposition of carbonates (inducing more production of metallic elements for creating new pores) and the erosion of carbon layer. Since Co and Fe have similar properties and chemical behaviors to those of Ni, a similar effect on the mesoporisty development can also be expected (as shown in Fig. 2).

The results obtained from temperature-programmed reductions are summarized in Fig. 3. In the case of BCNi catalysts, it is possible to observe that NiO reduction occurred between 500 and 600 °C. This observed behavior is in good agreement with earlier studies [32,49]. Furthermore, from the reduction profiles, it is evident that Ni loading had a marked influence on the reducibility properties, suggesting that the active metal dispersion had a non-negligible impact on Ni-biochar bond strength. Indeed, the α peak (low-temperature NiO reduction) appeared as a shoulder for the BCNi4 sample, while it was more evident for the BCNi7 sample and even more intense for the BCNi10 catalyst. For the latter, the intensity of the α peak was almost the same as that of the β reduction peak. This suggests that the higher the Ni loading, the higher the amount of low-interactive Ni sites on the biochar surface. Besides, the observed decrease in the reduction temperature at higher Ni loadings (which was previously reported by Nguyen et al. [50]) could be ascribed to NiO multilayers, which weakened the Ni-biochar interactions. Nevertheless, considering the low reduction temperature of unsupported NiO (325 °C [51]) it can be stated that all the Ni-based samples revealed a remarkable interaction between active metal and support.

Regarding the cobalt catalysts, it was observed that Co reduction occurred in series, describing two distinct reduction peaks corresponding to the consecutive reduction of Co_3O_4 to CoO and CoO to Co [52,53]. CeO_2 reduction occurred in two steps as well (the first one at ca 400 °C and the second one at ca 600 °C). The low temperature (i.e., below 500 °C) observed for the reduction of CeO_2 was somewhat unexpected. However, this finding could be related to the reducing activity of the BC support. Regarding the BCFe catalyst, it is well known that iron oxide commonly undergoes reduction in three steps,

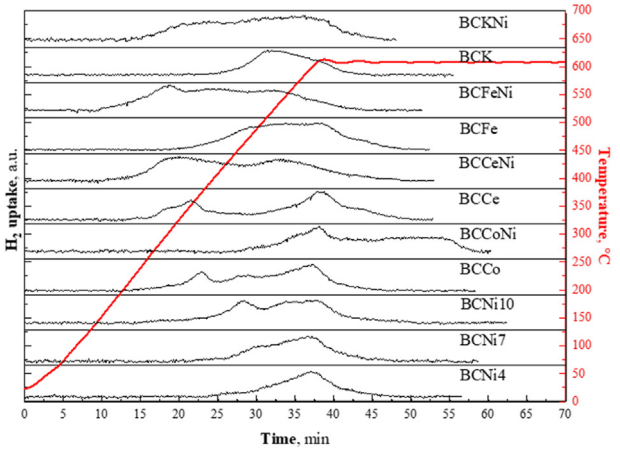

Fig. 3 – Temperature-programmed reduction results obtained for all the produced catalysts.

from Fe_2O_3 to Fe_3O_4, Fe_3O_4 to FeO, and FeO to Fe [36]. As can be seen in Fig. 3, the BCFe catalyst exhibited a broad reduction peak starting at approximately 300 °C. As mentioned above for the case of BCCe catalyst, iron oxides reduction was anticipated because of the interaction with the activated biochar support [54]. Finally, for the BCK catalyst, K_2O reduction was observed, as expected [55], at approximately 500 °C, suggesting that the BC support did not play any effect on the reduction of potassium oxide.

The bimetallic BCCeNi, BCFeNi, and BCKNi formulations demonstrated even more enhanced reducibility if compared to the respective monometallic samples. A possible explanation for this is that the higher amount of active species led to the formation of bulk oxides, which could be easily reduced. In addition, the increase in NiO reducibility in the presence of K_2O has previously been observed [56]. The bimetallic BCCoNi catalyst showed lower reducibility compared to that of the BCCo and BCNi10 samples. This might be due to the formation of a Co–Ni alloy, which has a higher bond strength than metals themselves [57]. This particular result would suggest that the active species in the BCCoNi dual catalyst have lower mobility; however, and despite its weaker reducibility, this could be beneficial for the reaction, especially in terms of catalyst stability.

Results from the CO_2-TPD measurements are detailed in Appendix A (Supplementary Material). The main outcomes showed that the addition of a metallic phase on the carbonaceous support resulted in the formation of new CO_2 chemisorption sites (see Fig. A1). Basic sites can be weak, medium or strong depending on the temperature at which CO_2 desorbed (100–150 °C, 150–250 °C, and above 250 °C; respectively). Since surface energies strongly depend on the metal specie, different metals can result in different basic sites [58]. In the present study, the introduction of Ni to the BCCo catalyst led to new medium and strong basic sites. This finding is in agreement with the previous studies by Nagban et al. [61] and Turap et al. [62], in which it was reported that the addition of Co to a Ni-based catalyst (supported on ZrO_2 and CeO_2) resulted in the formation of new strong basic sites. It is well known that catalysts having higher surface basicity are less prone to coke deposition and subsequent deactivation [63].

Steam reforming of acetic acid

Monometallic catalysts

Fig. 4a graphically summarizes the outcomes obtained from the steam reforming of acetic acid at 600 °C using the monometallic catalysts. The non-impregnated activated biochar (BC) showed a certain activity, but also a low stability, leading to a rapid decrease in the acetic acid conversion (X_{AcOH}). As mentioned above, BC was characterized by a high surface area and a high ash content. These two features, together with the carbon deposits produced via secondary reactions, could explain the certain catalytic activity of BC. Similar instability was also observed for the cobalt-, potassium- and cerium-based catalysts, which exhibited a pronounced deactivation after only a few minutes of run time. The BCFe catalyst showed a quite different performance. During the first 5 min, acetic acid was completely converted. After that, however, the catalyst activity decreased to a conversion value of 50%, which remained stable for the rest of the experiment.

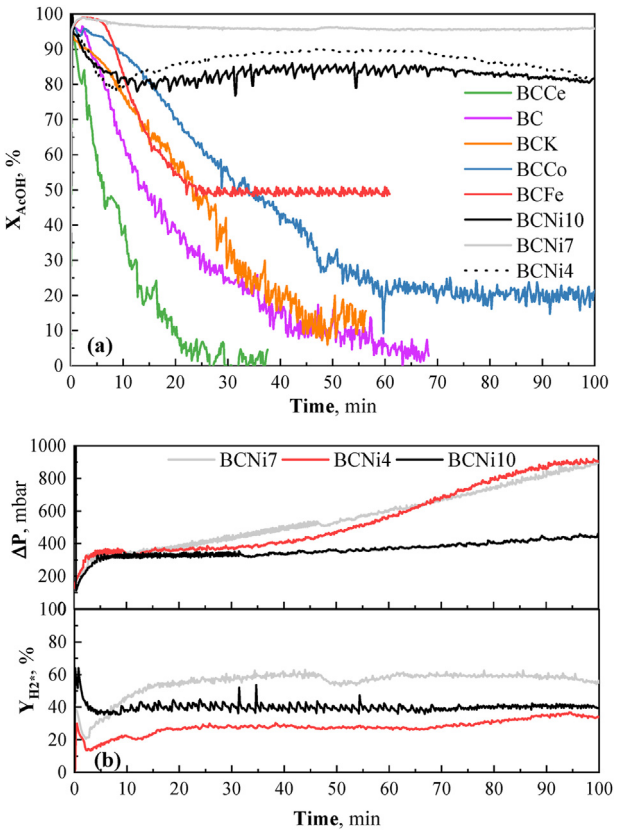

Fig. 4 – Results obtained from the steam reforming of acetic acid at 600 °C and 2.94 h^{-1}: Acetic acid conversion obtained with the monometallic catalysts (a); hydrogen yield and pressure drop evolution during the experiments involving the three nickel-based catalysts (b).

As can be seen in Fig. 4a, the nickel-based catalysts clearly exhibited the best performances in terms of acetic acid conversion and stability. The ability of nickel to break the C–O and C–H bonds is widely recognized in the literature [16,31,41,64], making this metal commonly employed in steam reforming processes. All the three Ni loadings showed high conversion values (80%–95%), which remained almost constant during the entire run time. In terms of conversion, it was clear that 7 wt % of nickel was the best formulation for our purpose. Nevertheless, from the pressure drop measurement across the bed (see Fig. 4b), it can be deduced a certain extent of coke deposition, which gradually clogged the catalytic bed. In particular, for BCNi4 and BCNi7 catalysts, which showed the highest conversion values, the highest coke deposition rates were observed. Therefore, these catalysts could be considered not suitable for long-time applications. For the catalyst having the highest nickel loading (BCNi10), an almost constant pressure drop value was observed, suggesting that the relatively high nickel content was able to hinder the deposition of coke on the catalyst. Moreover, from the evolutions of the hydrogen yield shown in Fig. 4b, it can be deduced that the BCNi10 catalysts exhibited a stable performance. Thus, it can be concluded that a 10 wt % of Ni loading

represents the most convenient alternative to simultaneously reach a good conversion towards hydrogen and good stability over time. This finding partly agrees with the results reported by Zhang et al. [65], who gave evidence that relatively low Ni loadings (i.e., below 10 wt %) in a Ni/Al_2O_3 catalyst led to relatively low catalytic activity and fast deactivation by coke deposition.

Bimetallic catalysts

This phase of the study was addressed to improve the overall performance of the BCNi10 catalyst. To this end, four bimetallic catalysts were produced by adding a 10 wt % of nickel to the BCK, BCCe, BCFe, and BCCo catalysts.

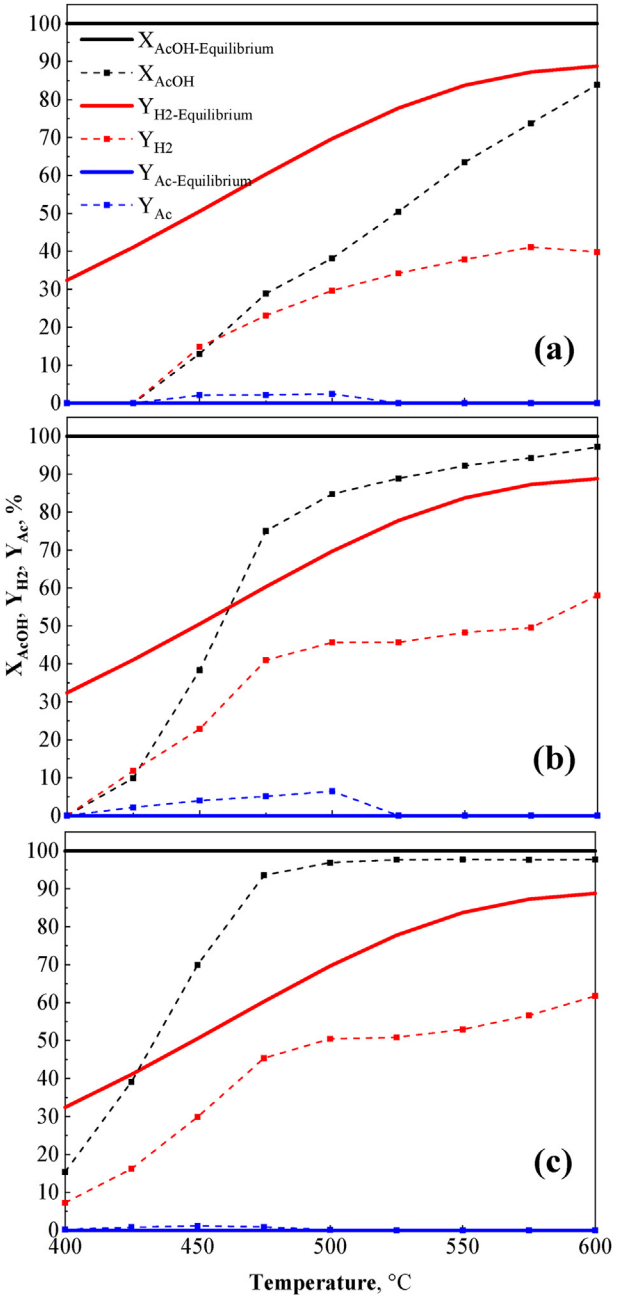

Fig. 5 – Experimental and theoretical equilibrium values of acetic acid conversion, H_2 yield, and acetone yield as a function of the bed temperature for different bimetallic catalysts: BCFeNi (a); BCCeNi (b); and BCCoNi (c).

Fig. 5 shows the results obtained for three of the four bimetallic catalysts during acetic acid steam reforming at different temperatures. Since the potassium-nickel catalyst (BCKNi) showed severe instability during the reforming test, which was comparable to that of BCK, the obtained outcomes for this catalyst are not reported herein. From the data shown in Fig. 5, it can be concluded that the addition of nickel to the tested monometallic catalysts was able to enhance their catalytic performance and stability. In the case of the iron-based catalysts (see Fig. 5a), for example, the acetic acid conversion at 600 °C increased by around 30% when the second metal phase (Ni) was added. Nevertheless, the results for the BCFeNi catalyst were similar to those obtained for the BCNi10 monometallic catalyst (Fig. 4a). For the BCCeNi catalyst (see Fig. 5b), however, the synergistic effect of cerium and nickel was more evident in view of the improved conversion and hydrogen yield (which increased by around 15% and 20%, respectively, compared to the monometallic BCNi10 catalyst). On the other hand, a decrease in the reactor temperature from 600 to 500 °C did not result in a substantial loss of catalytic activity of the BCCeNi catalyst. Nonetheless, at 500 °C and below, a higher production of acetone was observed, probably as a result of the ketonization of acetic acid [66].

Among the four bimetallic catalysts tested, the cobalt-nickel one (BCCoNi) resulted to be the most suitable for acetic acid steam reforming. In fact, as shown in Fig. 5c, the experimental conversion was close to the thermodynamic equilibrium value at 600 °C. The hydrogen yield decreased from 61% (at 600 °C) to 45% (at 475 °C). In any case, the decrease in the hydrogen yield at lower temperatures was not accompanied by an increase in the acetone yield, suggesting that the main reaction mechanisms were catalytic steam reforming and cracking for temperatures above 475 °C.

In light of the good results obtained for the BCCoNi catalyst, a long-time stability test (i.e., 750 min) was carried out at 600 °C. Results shown in Fig. 6a correspond to the sum of two consecutive runs. At the end of the first run (475 min), the pump was stopped and the reactor cooled down under N_2 to room temperature. The following experiment started when the reactor temperature reached again 600 °C. A conversion value above 90% was obtained during the first 250 min. After that, conversion decreased gradually. This deactivation could be ascribed to two different phenomena: (1) carbon deposition on the active sites and (2) formation of byproducts, which are strongly adsorbed on the catalytic sites. The latter assumption was confirmed by the results obtained during the second run. In fact, after the heating step under N_2, the catalyst was partially regenerated. Nevertheless, the conversion obtained with the fresh catalyst was not achieved again, probably due to a certain availability of coke on the surface.

An additional stability test was carried out changing the operating temperature. The run started at 600 °C until stabilization was reached; then, the system was cooled down to 500 °C (at 5 °C min^{-1}) and the conditions were kept for 15 min. After that, the system was cooled down to 400 °C, at the same cooling rate, and kept at this temperature for 15 min. Finally, the system was then heated up to 600 °C. As shown in Fig. 6b, both the conversion and hydrogen yield remained reasonably

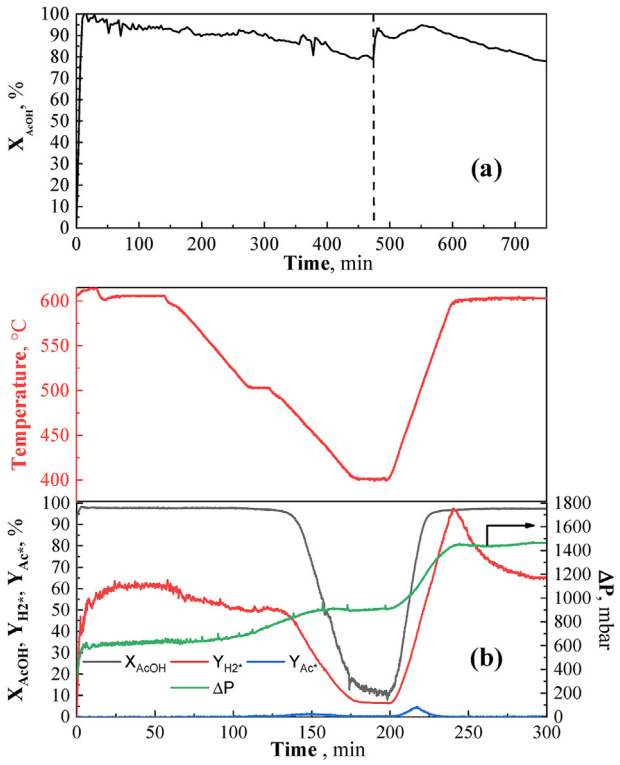

Fig. 6 – Stability test of BCCoNi catalyst for steam reforming of acetic acid: 2-step stability test performed at 600 °C (a); and cycling stability test carried out in the range of 400–600 °C (b).

stable in the range of 475–600 °C and were coherent to the outcomes displayed in Fig. 5c. The pressure drop across the bed remained almost constant during the first isothermal phase and started to increase when the temperature began to fall, due to the higher extent of coke formation. In addition, a certain production of acetone was also observed during the cooling down stage [8]. When the experimental device was heated up again to 600 °C, the conversion of acetic acid reached the same value as that of the first stage, indicating negligible catalyst deactivation. For its part, the hydrogen yield achieved a transient peak of 95% and then settled back to a stable plateau of 65%. Similar behavior was observed for the acetone yield. Since the observed increases in the production of both hydrogen and acetone were not accompanied by an increase in the reactant conversion, one can hypothesize that a considerable fraction of these compounds was previously adsorbed on the catalyst surface and then released with the increase in temperature, confirming the double nature of the deactivation mechanism.

Based on the above-explained results, one can conclude that the dual Ni–Co biochar-supported catalyst was suitable for acetic acid steam reforming applications. In particular, it was possible to obtain excellent performances comparable to those obtained for commonly used supports, such as Al_2O_3 and SBA [16,67–69].

Steam reforming of a mixture of acetic acid, acetone, ethanol, and eugenol

Once identified the most promising metal/BC catalyst (BCCoNi), research was focused on assessing the effect of the operating conditions on the overall performance of the steam reforming of a model mixture composed of acetone, acetic acid, ethanol, eugenol, and water (S/C = 4). Previous studies reported that acetone, ethanol, and acetic acid could easily be reformed over a Ni- or Co-based catalyst [8,67,70–72]. To the best of our knowledge, no studies concerning the steam reforming of eugenol (a phenolic compound) have been published so far.

From the results obtained for the steam reforming at 600 °C, which are shown in Fig. 7a, it can be observed that carbon conversion (X_c) rapidly decreased from an initial value of 50% to an almost constant value of ca. 30%. This behavior was similar to that observed for the BCFe catalyst for the acetic acid steam reforming. The similarity between the obtained hydrogen and carbon dioxide yields (see Fig. 7a) seems to suggest that the steam reforming was the main reaction involved. Despite the relatively low conversion attained at steady-state, the products selectivity remained relatively constant during the entire experiment (see Fig. 7b), indicating that the catalyst deactivation did not result in significant changes in the reforming mechanism. More in detail, the low yields of both CO and CH_4 (below 10%), could suggest a relatively low extent of both the reverse Boudouard and decomposition reactions, respectively [73–75]. As it can be deduced from a reference experiment, which was conducted using only activated biochar as catalytic bed (see Fig. A2), it seems clear that steam reforming reactions only took place at the surface of metal nanoparticles. On the other hand, Fig. A3 displays the product evolution measured for a catalytic test, which was conducted at a LHSV of 2.94 h^{-1}, 600 °C and using a relatively high flow (the double than that used previously) of the carrier gas (N_2). This experiment was aimed at assessing the influence of the partial pressure of the reactant. For this test, we expected a decrease in the overall performance of the catalyst but a better stability. Nevertheless, the results showed an even faster deactivation, which could be directly related to the water partial pressure. Probably, during the previous experiment (which corresponds to Fig. 7a), the higher water content was able to hinder the coke deposition or, at least, to gasify part of the carbon deposits on the catalyst surface, leading to a decrease in the deactivation rate.

To further improve the catalytic performances, a study on the influence of the operating temperature and liquid hourly space velocity was carried out. Fig. A4 shows the carbon conversions obtained at different temperatures in the range of 500–600 °C and the corresponding equilibrium values (at a constant LHSV of 2.94 h^{-1}). Even though the conversion of the reactant was thermodynamically promoted, our configuration only allowed us to reach a maximum carbon conversion of 30%.

When the liquid residence time was set at 5.88 h^{-1}, a drastic reduction of the carbon conversion was observed (see Fig. 8a). Conversely, when the lowest LHSV value (1.47 h^{-1}) was used, the performance of the catalyst was slightly improved with respect to the initial condition (i.e., 2.94 h^{-1}).

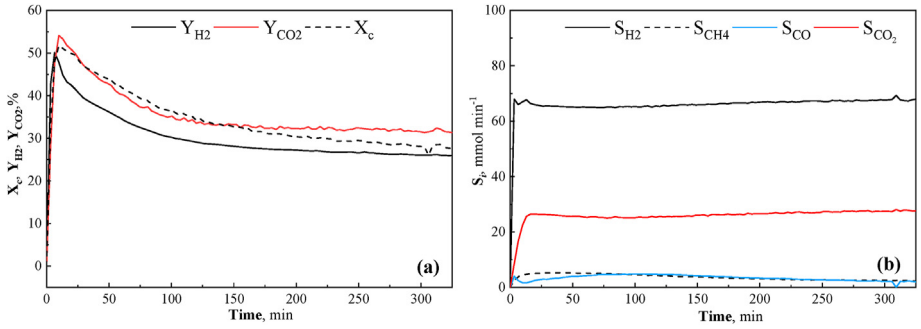

Fig. 7 – Test of BCCoNi catalyst for steam reforming of the model mixture at 600 °C and 2.94 h^{-1}: carbon conversion, hydrogen and carbon dioxide yields (a); and products selectivity (b).

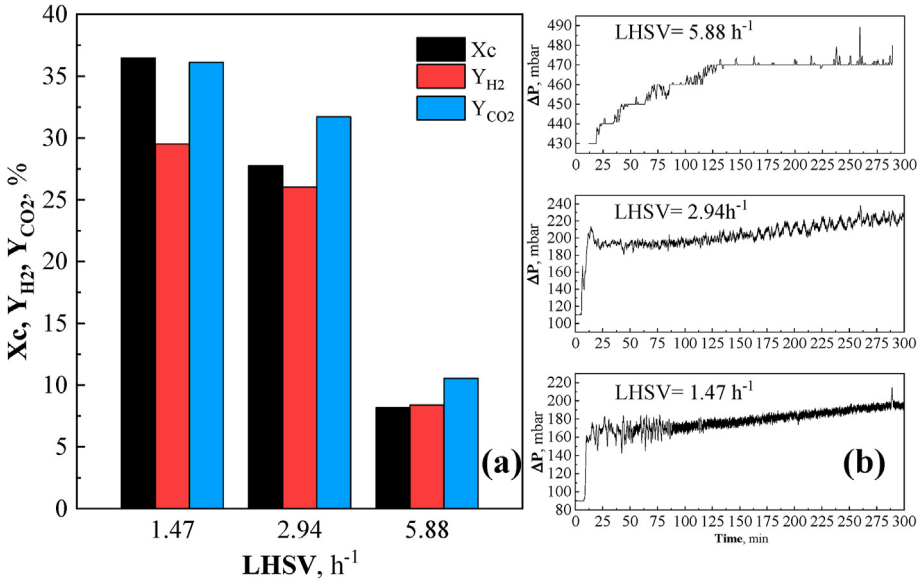

Fig. 8 – Outcomes in terms of X_c, Y_{H2}, and Y_{CO2} (a) and pressure drops evolution (b) obtained for the study of the influence of LHSV on the reforming of the model mixture at 600 °C using BCCoNi as catalyst.

The fast deactivation observed during the early stage of the experiment (see Fig. 7) could be ascribed to different mechanisms: (1) sintering of the metal phases [76], (2) oxidation of the metal active phase [10,77], (3) gasification of the support [78], (4) coke deposition [16,17]; and (5) catalyst poisoning [15,41]. Sintering of the active phases is strictly related to the operating temperature and to the reaction environment [79]. Since the experiments involving acetic acid (where fast deactivation was not deduced from Fig. 6) and the model mixture were conducted under similar conditions, we can hypothesize that sintering does not explain the observed deactivation. To verify if the deactivation was due to active phase oxidation, the spent catalyst was reduced and tested again under the same conditions. The results obtained did not show the activity peak detected when the fresh catalyst was firstly tested. Therefore, the oxidation of the metal phase could also be ruled out. Gasification of the carbon matrix caused by the water available in the liquid feed mixture could lead to a modification of the support structure with subsequent loss of active phase. However, a test employing only BC as catalytic bed was performed feeding only water along with N_2 at 600 °C and monitoring the gas outlet stream compositions. Results from this test revealed an almost negligible occurrence of the steam gasification reaction. In summary, it could be concluded that the deactivation was mainly caused by coke deposition or catalyst poisoning during the first minutes of the catalytic test.

The nature of coke could be distinguished between filamentous and amorphous, with the latter being responsible for the catalytic activity loss due to encapsulation of the metallic phase [80–82]. This kind of deactivation is particularly significant in the case of microporous materials since the smaller pores are the first ones to be filled by coke [83,84]. However, and in light of the similar pressure drops measured at the three LHSV values (see Fig. 8b), a relatively good dispersion of the metal phases (which could hinder carbon deposition [85]) can be assumed. Therefore, the observed fast deactivation should mainly be ascribed to the production of relatively heavy organic compounds, which could be adsorbed on the active sites, and

subsequently react to form more stable and not easily desorbable reaction intermediates. In line with this, Zhang et al. [15] reported that the strong adsorption of phenolic compounds on a Ni/Al_2O_3 catalyst could explain the observed low catalytic activity in steam reforming of guaiacol. In the present study, the poisoning of catalyst could eventually reach a quasi-steady-state after 100 min (see Fig. 7a), in which the fraction of available catalytic sites could remain constant.

Steam reforming of slow pyrolysis oil

Even though the BCCoNi catalyst showed a modest catalytic activity for the steam reforming of the model mixture, its stability at steady-state was encouraging. Therefore, the catalytic activity of this catalyst was also evaluated for the steam reforming of a real slow pyrolysis bio-oil, which had a mean empirical formula of $CH_{2.34}O_{0.88}$ and a water content of 71 wt % (S/C = 3.87). No sulfur, which could irreversibly poison the catalyst [86], was detected in the bio-oil.

The results obtained from the catalytic test using the above-mentioned pyrolysis oil were clearly unsatisfactory, as shown in Fig. A5. After a few minutes of run time, the catalytic activity drastically dropped to a value comparable to that obtained for the model mixture and using only the BC support as catalytic bed. Such behavior could probably be ascribed to the sugar-type compounds present in the pyrolysis oil. Paasikallio et al. [37] identified a 4.3 wt % of levoglucosan in a forest thinnings-derived oil. These compounds, which are non-volatile and undergo thermal decomposition rather than vaporization, can produce charring matter, which unavoidably covers the catalyst surface [87]. Furthermore, the presence of such compounds caused numerous clogs in the evaporation system of the experimental setup, even at low temperatures (150–250 °C). To avoid the above-mentioned issues, the raw pyrolysis oil was distilled at atmospheric pressure and 200 °C in order to obtain a lighter fraction, free of sugar-type compounds. The obtained distillate had an empirical formula of $CH_{2.42}O_{0.75}$ and a water content of 85 wt % (S/C = 8.32).

The effects of LHSV on the carbon conversion and products selectivity (using the distilled fraction of pyrolysis oil at a constant temperature of 600 °C) are summarized graphically in Fig. 9a. In contrast to the outcomes previously reported for the model mixture, an increase in reactants residence time led to a marked increase in the carbon conversion up to 45%. Regardless of the value of LHSV, hydrogen was always the most abundant product, followed by CO_2. CH_4 could be produced by methanation of CO and CO_2 or, more probably, by thermal decomposition of reactants.

Fig. 9b reports the conversion and selectivity values obtained at different operating temperatures (at a constant LHSV of 2.94 h^{-1}). An increase from 550 to 700 °C led to a marked increase in the carbon conversion, whereas a further increase from 700 to 750 °C resulted in a slight enhancement of the reactant conversion. In the range of 600–750 °C, the temperature did not significantly affect the distribution of products. This suggests that the operating temperature only influenced the process from a kinetic point of view, without affecting the main reaction mechanism.

A stability test was also performed for the steam reforming of the distilled pyrolysis oil under the previously-identified optimal conditions (700 °C and 1.47 h^{-1}). The evolution of the conversion, products selectivity, and pressure drop across the bed are shown in Fig. 10. The stability test was divided into two separate runs. At the end of the first one (vertical dashed line in Fig. 10) the pump was stopped. The reactor was then cooled down to 20 °C and heated up again to 700 °C under N_2.

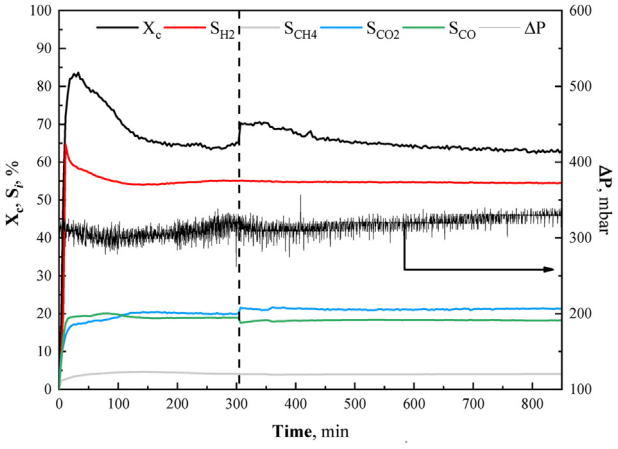

Fig. 10 – 2-Step long-term stability test for the BCCoNi catalyst during the steam reforming of distilled pyrolysis oil at 700 °C and 1.47 h^{-1}.

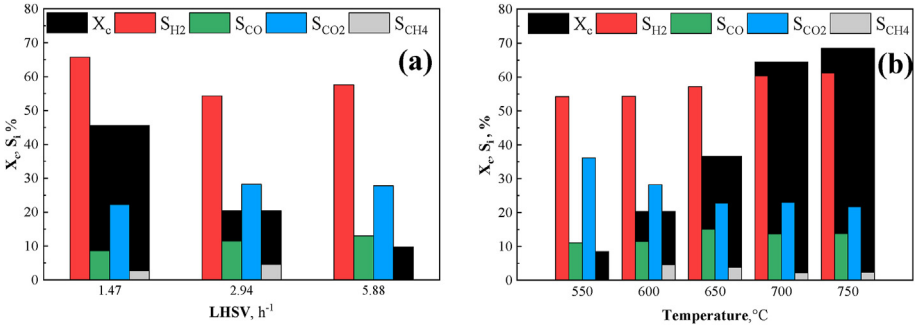

Fig. 9 – Results in terms of carbon conversion and products selectivity obtained during the steam reforming of distilled pyrolysis oil: at constant temperature (600 °C) and different LHSV values (a); and at different temperatures and constant LHSV of 2.94 h^{-1} (b).

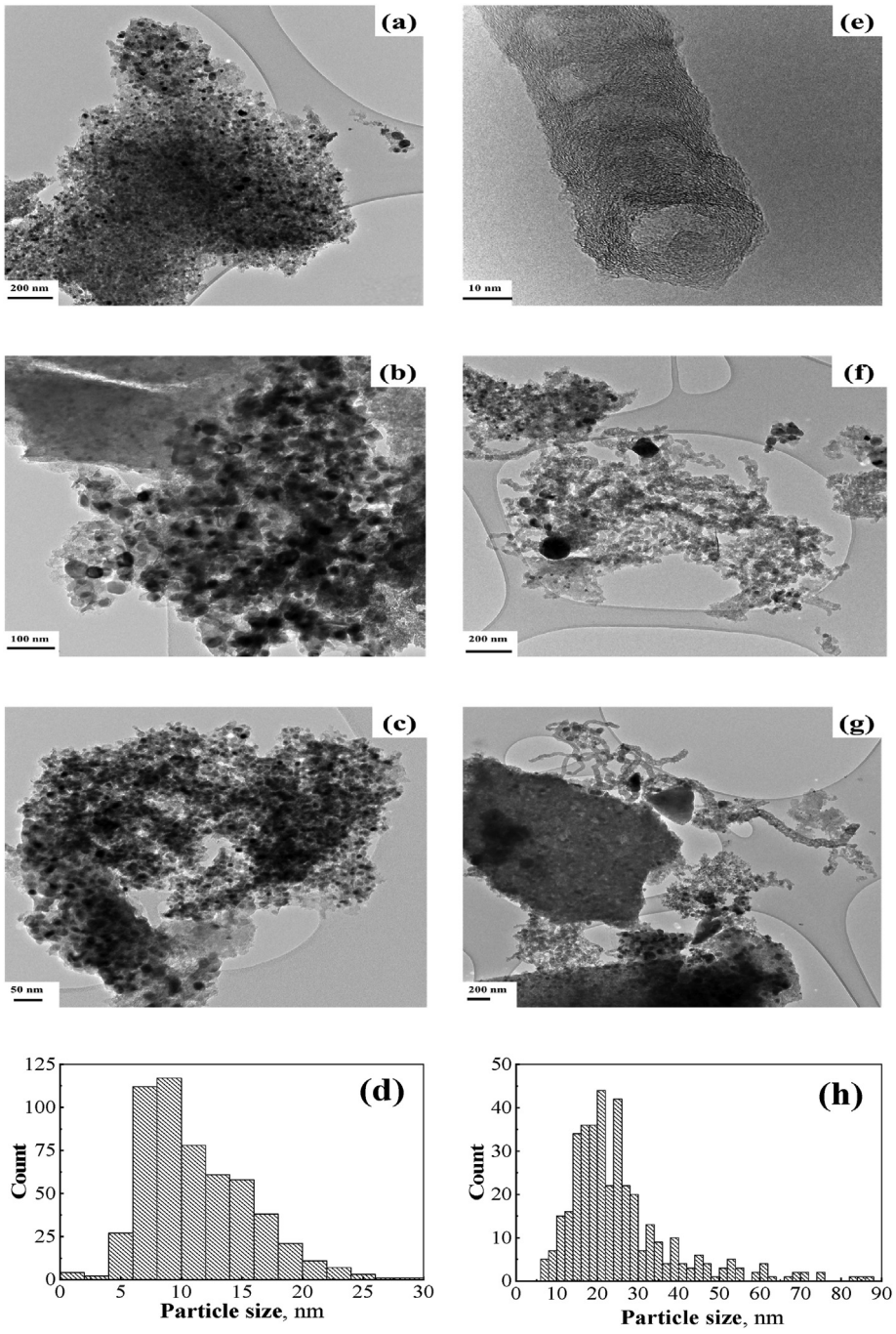

Fig. 11 – TEM images and metal particle size distribution of fresh (a, b, c, d) and spent (e, f, g, h) BCCoNi catalyst used in steam reforming of distilled pyrolysis oil at 700 °C and 1.47 h^{-1}.

Once the reactor reached the setpoint, the distilled oil was then fed into the system. As can be seen in Fig. 10, and similarly to that observed for the model mixture, the conversion reached a transient peak (84%) and then rapidly decreased to an almost constant value (65%). The thermal treatment under nitrogen slightly regenerated the catalyst, confirming the presence of heavier compounds adsorbed on the solid surface. As observed for the steam reforming of both the acetic acid and model mixture, the pressure drop remained reasonably constant, suggesting that the possible coke deposition did not lead to a deactivation of the catalyst. The yields of gaseous species remained almost constant during the whole experiment. The main difference between the results shown in Figs. 6a and 10 was that, in the first case, the conversion did not stabilize to a constant value; however, in the case of pyrolysis oil, a stable value (plateau) was achieved after 150 min. Such value remained constant even after the thermal regeneration of the catalyst.

Fig. 11 shows the TEM images of both the fresh and spent BCCoNi catalyst. From Fig. 11d and h, it can be seen that the size of metal nanoparticles was larger for the spent catalyst. This could be explained by sintering phenomena, leading to

the formation of larger clusters (black agglomerates in Fig. 11f). Nevertheless, the observed sintering of the activate phase did not result in an evident loss of catalytic activity. Furthermore, carbon nanotubes with an internal diameter of ca. 20 nm (see Fig. 11e) were observed on the surface of the spent catalyst [88,89]. Their presence could be attributed to the decomposition of guaiacols and furfurals, which, due to their aromatic structure, could promote the formation of this kind of carbon nanostructures [90,91].

Conclusions

In view of the results reported in the present study, the following conclusions can be drawn:

1. Physically activated (at mild temperature and moderate pressure) wheat straw-derived biochar appears as a promising support material for heterogeneous metal-based catalysts. Among the five metallic active phases tested for the steam reforming of acetic acid, nickel resulted to be the best choice. In particular, a Ni loading of 10 wt % showed a good tradeoff between acetic acid conversion and resistance to deactivation. Furthermore, the addition of a second metallic phase (i.e., 7 wt % of cobalt) greatly improved the catalyst activity and stability.
2. The bimetallic Co–Ni-based catalyst was also tested for steam reforming of a pyrolysis oil model mixture containing water, acetone, ethanol, acetic acid, and eugenol. Results showed a severe catalyst deactivation after a few minutes of run time, where conversion decreased from 50% to a steady value of 30%. This could be attributed to catalyst poisoning caused by the adsorption of relatively heavy compounds derived from the decomposition of eugenol.
3. Due to the presence of sugar-derived compounds, which led to a rapid deactivation of the catalyst, the real slow pyrolysis was distilled in order to be tested in steam reforming experiments. For this liquid feed, it was possible to obtain a total carbon conversion of 65% and a selectivity toward hydrogen of 55% by properly setting the operating conditions (temperature and liquid space velocity). A 2-step long-time stability test revealed that, despite the presence of heavier organic compounds adsorbed on the catalyst, both the conversion and hydrogen yield remained reasonably constant over time, indicating good stability of the catalyst. Further investigations will be required to further fine-tuning the operating conditions and evaluate the performance of the catalysts for even longer periods of time.

Declaration of competing interest

The authors declare that they have no known competing financial interests or personal relationships that could have appeared to influence the work reported in this paper.

Acknowledgments

This project received funding from the European Union's Horizon 2020 research and innovation programme under the Marie Skłodowska-Curie grant agreement No 721991. The authors also acknowledge the funding from the Aragón Government (Ref. T22_20R), co-funded by FEDER 2014–2020 "Construyendo Europa desde Aragón". The authors gratefully thank José Antonio Manso and Olga Marín for their help in the preparation and characterization of the samples. Authors would like to acknowledge the use of Servicio General de Apoyo a la Investigación-SAI, Universidad de Zaragoza.

Nomenclature

d_p	Pore diameter (nm)
F_c	Carbon molar flow rate (mol min^{-1})
F_i	Products molar flow rate (mol min^{-1})
F_{iEq}	Products molar flow rate at equilibrium conditions (mol min^{-1})
Q_{mix}	Volume flow rate of the liquid blend (mL h^{-1})
S/C	Steam to carbon molar ratio
S_i	Product selectivity (%)
S_L	Langmuir surface area (m^2 g^{-1})
V_{cat}	Catalyst volume (mL)
V_{meso}	Volume of mesopores (cm^3 g^{-1})
V_{micro}	Volume of micropores (cm^3 g^{-1})
V_{tot}	Total pore volume (cm^3 g^{-1})
X_{AcOH}	Acetic acid conversion in acetic acid steam reforming (%)
X_c	Carbon conversion (%)
Y_{Ac*}	Acetone yield in acetic acid steam reforming (%)
Y_{H2*}	Hydrogen yield in acetic acid steam reforming (%)
Y_i	Product yield (%)

Acronyms

AcOH	Acetic Acid
CHN	Ultimate analysis
CO_2-TPD	CO_2 temperature programmed desorption
DRIFT	Diffuse reflectance *infrared* fourier transform spectroscopy
LHSV	Liquid hourly space velocity; LHSV = Q_{mix} V_{cat}^{-1}
NLDFT	Non-local density functional theory
PSD	Pore size distribution
TCD	Thermal conductivity detector
TEM	Transmission electron microscopy
TPR	Temperature programmed reduction
XRF	X-ray fluorescence spectroscopy
μ-GC	Micro gas chromatograph

Appendix A. Supplementary data

Supplementary data to this article can be found online at https://doi.org/10.1016/j.ijhydene.2021.05.193.

REFERENCES

[1] Gentile G, Debiagi PEA, Cuoci A, Frassoldati A, Ranzi E, Faravelli T. A computational framework for the pyrolysis of anisotropic biomass particles. Chem Eng J 2017;321:458–73. https://doi.org/10.1016/j.cej.2017.03.113.

[2] Debiagi P, Gentile G, Cuoci A, Frassoldati A, Ranzi E, Faravelli T. A predictive model of biochar formation and characterization. J Anal Appl Pyrolysis 2018;134:326–35. https://doi.org/10.1016/j.jaap.2018.06.022.

[3] Anca-Couce A, Scharler R. Modelling heat of reaction in biomass pyrolysis with detailed reaction schemes. Fuel 2017;206:572–9. https://doi.org/10.1016/j.fuel.2017.06.011.

[4] Xiu S, Shahbazi A. Bio-oil production and upgrading research: a review. Renew Sustain Energy Rev 2012;16:4406–14. https://doi.org/10.1016/j.rser.2012.04.028.

[5] Santamaria L, Lopez G, Arregi A, Amutio M, Artetxe M, Bilbao J, et al. Influence of the support on Ni catalysts performance in the in-line steam reforming of biomass fast pyrolysis derived volatiles. Appl Catal B Environ 2018;229:105–13. https://doi.org/10.1016/j.apcatb.2018.02.003.

[6] Phongprueksathat N, Meeyoo V, Rirksomboon T. Steam reforming of acetic acid for hydrogenproduction : catalytic performances of Ni and Co supported on Ce0·75Zr0·25O2 catalysts. Int J Hydrogen Energy 2019;44:9359–67. https://doi.org/10.1016/j.ijhydene.2019.02.085.

[7] Sueyasu T, Oike T, Mori A, Kudo S, Norinaga K, Hayashi JI. Simultaneous steam reforming of tar and steam gasification of char from the pyrolysis of potassium-loaded woody biomass. Energy Fuels 2012;26:199–208. https://doi.org/10.1021/ef201166a.

[8] Hu X, Lu G. Investigation of the steam reforming of a series of model compounds derived from bio-oil for hydrogen production. Appl Catal B Environ 2009;88:376–85. https://doi.org/10.1016/j.apcatb.2008.10.021.

[9] Trane-Restrup R, Jensen AD. Steam reforming of cyclic model compounds of bio-oil over Ni-based catalysts: product distribution and carbon formation. Appl Catal B Environ 2015;165:117–27. https://doi.org/10.1016/j.apcatb.2014.09.026.

[10] Augusto BL, Ribeiro MC, Aires FJCS, da Silva VT, Noronha FB. Hydrogen production by the steam reforming of ethanol over cobalt catalysts supported on different carbon nanostructures. Catal Today 2020;344:66–74. https://doi.org/10.1016/j.cattod.2018.10.029.

[11] Vagia EC, Lemonidou AA. Hydrogen production via steam reforming of bio-oil components over calcium aluminate supported nickel and noble metal catalysts. Appl Catal Gen 2008;351:111–21. https://doi.org/10.1016/j.apcata.2008.09.007.

[12] Shen Y, Zhao P, Shao Q, Takahashi F, Yoshikawa K. In situ catalytic conversion of tar using rice husk char/ash supported nickel-iron catalysts for biomass pyrolytic gasification combined with the mixing-simulation in fluidized-bed gasifier. Appl Energy 2015;160:808–19. https://doi.org/10.1016/j.apenergy.2014.10.074.

[13] Song H, Zhang L, Watson RB, Braden D, Ozkan US. Investigation of bio-ethanol steam reforming over cobalt-based catalysts. Catal Today 2007;129:346–54. https://doi.org/10.1016/j.cattod.2006.11.028.

[14] Lin SSY, Kim DH, Ha SY. Metallic phases of cobalt-based catalysts in ethanol steam reforming: the effect of cerium oxide. Appl Catal Gen 2009;355:69–77. https://doi.org/10.1016/j.apcata.2008.11.032.

[15] Zhang Z, Hu X, Zhang L, Yang Y, Li Q, Fan H, et al. Steam reforming of guaiacol over Ni/Al2O3 and Ni/SBA-15: impacts of support on catalytic behaviors of nickel and properties of coke. Fuel Process Technol 2019;191:138–51. https://doi.org/10.1016/j.fuproc.2019.04.001.

[16] An L, Dong C, Yang Y, Zhang J, He L. The influence of Ni loading on coke formation in steam reforming of acetic acid. Renew Energy 2011;36:930–5. https://doi.org/10.1016/j.renene.2010.08.029.

[17] Coll R, Salvadó J, Farriol X, Montané D. Steam reforming model compounds of biomass gasification tars: conversion at different operating conditions and tendency towards coke formation. Fuel Process Technol 2001;74:19–31. https://doi.org/10.1016/S0378-3820(01)00214-4.

[18] Chen J, Sun J, Wang Y. Catalysts for steam reforming of bio-oil: a review. Ind Eng Chem Res 2017;56:4627–37. https://doi.org/10.1021/acs.iecr.7b00600.

[19] Xiong X, Yu IKM, Cao L, Tsang DCW, Zhang S, Ok YS. A review of biochar-based catalysts for chemical synthesis, biofuel production, and pollution control. Bioresour Technol 2017;246:254–70. https://doi.org/10.1016/j.biortech.2017.06.163.

[20] Qian K, Kumar A, Zhang H, Bellmer D, Huhnke R. Recent advances in utilization of biochar. Renew Sustain Energy Rev 2015;42:1055–64. https://doi.org/10.1016/j.rser.2014.10.074.

[21] Lee J, Kim KH, Kwon EE. Biochar as a catalyst. Renew Sustain Energy Rev 2017;77:70–9. https://doi.org/10.1016/j.rser.2017.04.002.

[22] Dufour A, Celzard A, Fierro V, Martin E, Broust F, Zoulalian A. Catalytic decomposition of methane over a wood char concurrently activated by a pyrolysis gas. Appl Catal Gen 2008;346:164–73. https://doi.org/10.1016/j.apcata.2008.05.023.

[23] Shen Y. Chars as carbonaceous adsorbents/catalysts for tar elimination during biomass pyrolysis or gasification. Renew Sustain Energy Rev 2015;43:281–95. https://doi.org/10.1016/j.rser.2014.11.061.

[24] Manyà JJ, Azuara M, Manso JA. Biochar production through slow pyrolysis of different biomass materials: seeking the best operating conditions. Biomass Bioenergy 2018;117:115–23. https://doi.org/10.1016/j.biombioe.2018.07.019.

[25] Shan R, Han J, Gu J, Yuan H, Luo B, Chen Y. A review of recent developments in catalytic applications of biochar-based materials. Resour Conserv Recycl 2020;162:105036. https://doi.org/10.1016/j.resconrec.2020.105036.

[26] Di Stasi C, Alvira D, Greco G, González B, Manyà JJ. Physically activated wheat straw-derived biochar for biomass pyrolysis vapors upgrading with high resistance against coke deactivation. Fuel 2019;255:115807. https://doi.org/10.1016/j.fuel.2019.115807.

[27] Liu WJ, Jiang H, Yu HQ. Development of biochar-based functional materials: toward a sustainable platform carbon. Material. Chem Rev 2015;115:12251–85. https://doi.org/10.1021/acs.chemrev.5b00195.

[28] Di Stasi C, Greco G, Canevesi RLS, Izquierdo MT, Fierro V, Celzard A, et al. Influence of activation conditions on textural properties and performance of activated biochars for pyrolysis vapors upgrading. Fuel 2020:119759. https://doi.org/10.1016/j.fuel.2020.119759.

[29] Lee J, Kim KH, Kwon EE. Biochar as a catalyst. Renew Sustain Energy Rev 2017;77:70–9. https://doi.org/10.1016/j.rser.2017.04.002.

[30] Buentello-Montoya D, Zhang X, Li J, Ranade V, Marques S, Geron M. Performance of biochar as a catalyst for tar steam reforming: effect of the porous structure. Appl Energy 2020;259:114176. https://doi.org/10.1016/j.apenergy.2019.114176.

[31] Quan C, Wang H, Gao N. Development of activated biochar supported Ni catalyst for enhancing toluene steam reforming. Int J Energy Res 2020;44:5749–64. https://doi.org/10.1002/er.5335.

[32] Wang Y, Zhang Z, Zhang S, Wang Y, Hu S, Xiang J, et al. Steam reforming of acetic acid over Ni/biochar catalyst treated with HNO3: impacts of the treatment on surface properties and catalytic behaviors. Fuel 2020;278:118341. https://doi.org/10.1016/j.fuel.2020.118341.
[33] Greco G, Di Stasi C, Rego F, González B, Manyà JJ. Effects of slow-pyrolysis conditions on the products yields and properties and on exergy efficiency: a comprehensive assessment for wheat straw. Appl Energy 2020;279:115842. https://doi.org/10.1016/j.apenergy.2020.115842.
[34] Greco G, Videgain M, Di Stasi C, González B, Manyà JJ. Evolution of the mass-loss rate during atmospheric and pressurized slow pyrolysis of wheat straw in a bench-scale reactor. J Anal Appl Pyrolysis 2018;136:18–26. https://doi.org/10.1016/j.jaap.2018.11.007.
[35] Song X, Li K, Wang C, Sun X, Ning P, Tang L. Regeneration performance and mechanism of modified walnut shell biochar catalyst for low temperature catalytic hydrolysis of organic sulfur. Chem Eng J 2017;330:727–35. https://doi.org/10.1016/j.cej.2017.08.016.
[36] Wan HJ, Wu BS, Zhang CH, Xiang HW, Li YW, Xu BF, et al. Study on Fe-Al2O3 interaction over precipitated iron catalyst for Fischer-Tropsch synthesis. Catal Commun 2007;8:1538–45. https://doi.org/10.1016/j.catcom.2007.01.002.
[37] Paasikallio V, Kihlman J, Sánchez CA, Simell P, Solantausta Y, Lehtonen J. Steam reforming of pyrolysis oil aqueous fraction obtained by one-step fractional condensation. Int J Hydrogen Energy 2015;40:3149–57. https://doi.org/10.1016/j.ijhydene.2015.01.025.
[38] Cakiryilmaz N, Arbag H, Oktar N, Dogu G, Dogu T. Catalytic performances of Ni and Cu impregnated MCM-41 and Zr-MCM-41 for hydrogen production through steam reforming of acetic acid. Catal Today 2019;323:191–9. https://doi.org/10.1016/j.cattod.2018.06.004.
[39] Fu P, Zhang A, Luo S, Yi W, Hu S, Zhang Y. Catalytic steam reforming of biomass-derived acetic acid over two supported Ni catalysts for hydrogen-rich syngas production. ACS Omega 2019;4:13585–93. https://doi.org/10.1021/acsomega.9b01985.
[40] Lozano P, Simón A, García L, Ruiz J, Oliva M, Arauzo J. Influence of the Ni-Co/Al-Mg catalyst loading in the continuous aqueous phase reforming of the bio-oil aqueous fraction. Processes 2021;9:81. https://doi.org/10.3390/pr9010081.
[41] Zhang Z, Zhang X, Zhang L, Wang Y, Li X, Zhang S, et al. Steam reforming of guaiacol over Ni/SiO2 catalyst modified with basic oxides: impacts of alkalinity on properties of coke. Energy Convers Manag 2020;205:112301. https://doi.org/10.1016/j.enconman.2019.112301.
[42] Ma Z, Xiao R, Zhang H. Catalytic steam reforming of bio-oil model compounds for hydrogen-rich gas production using bio-char as catalyst. Int J Hydrogen Energy 2017;42:3579–85. https://doi.org/10.1016/j.ijhydene.2016.11.107.
[43] Jiang L, Hu S, Wang Y, Su S, Sun L, Xu B, et al. Catalytic effects of inherent alkali and alkaline earth metallic species on steam gasification of biomass. Int J Hydrogen Energy 2015;40:15460–9. https://doi.org/10.1016/j.ijhydene.2015.08.111.
[44] Wang Y, Zhang Z, Zhang S, Wang Y, Hu S, Xiang J, et al. Steam reforming of acetic acid over Ni/biochar catalyst treated with HNO3: impacts of the treatment on surface properties and catalytic behaviors. Fuel 2020;278:118341. https://doi.org/10.1016/j.fuel.2020.118341.
[45] Ji Y, Zhao Z, Duan A, Jiang G, Liu J. Comparative study on the formation and reduction of bulk and Al 2O3-supported cobalt oxides by H2-TPR technique. J Phys Chem C 2009;113:7186–99. https://doi.org/10.1021/jp8107057.
[46] Melnikov P, Nascimento VA, Arkhangelsky IV, Zanoni Consolo LZ, De Oliveira LCS. Thermal decomposition mechanism of iron(III) nitrate and characterization of intermediate products by the technique of computerized modeling. J Therm Anal Calorim 2014;115:145–51. https://doi.org/10.1007/s10973-013-3339-1.
[47] Brockner W, Ehrhardt C, Gjikaj M. Thermal decomposition of nickel nitrate hexahydrate, Ni(NO3)2·6H2O, in comparison to Co(NO3)2·6H2O and Ca(NO3)2·4H2O. Thermochim Acta 2007;456:64–8. https://doi.org/10.1016/j.tca.2007.01.031.
[48] Li D, Zhao L, Cao X, Xiao Z, Nan H, Qiu H. Nickel-catalyzed formation of mesoporous carbon structure promoted capacitive performance of exhausted biochar. Chem Eng J 2021;406:126856. https://doi.org/10.1016/j.cej.2020.126856.
[49] Chen J, Wang M, Wang S, Li X. Hydrogen production via steam reforming of acetic acid over biochar-supported nickel catalysts. Int J Hydrogen Energy 2018;43:18160–8. https://doi.org/10.1016/j.ijhydene.2018.08.048.
[50] Nguyen HKD, Pham VV, Do HT. Preparation of Ni/biochar catalyst for hydrotreating of bio-oil from microalgae biomass. Catal Lett 2016;146:2381–91. https://doi.org/10.1007/s10562-016-1873-8.
[51] Martínez R, Romero E, Guimon C, Bilbao R. CO2 reforming of methane over coprecipitated Ni-Al catalysts modified with lanthanum. Appl Catal Gen 2004;274:139–49. https://doi.org/10.1016/j.apcata.2004.06.017.
[52] Taghavi S, Tavasoli A, Asghari A, Signoretto M. Loading and promoter effects on the performance of nitrogen functionalized graphene nanosheets supported cobalt Fischer-Tropsch synthesis catalysts. Int J Hydrogen Energy 2019;44:10604–15. https://doi.org/10.1016/j.ijhydene.2019.03.015.
[53] de Barros Dias Moreira J, Bastos de Rezende D, Márcia Duarte Pasa V. Deoxygenation of Macauba acid oil over Co-based catalyst supported on activated biochar from Macauba endocarp: a potential and sustainable route for green diesel and biokerosene production. Fuel 2020;269:117253. https://doi.org/10.1016/j.fuel.2020.117253.
[54] Chew LM, Kangvansura P, Ruland H, Schulte HJ, Somsen C, Xia W, et al. Effect of nitrogen doping on the reducibility, activity and selectivity of carbon nanotube-supported iron catalysts applied in CO2 hydrogenation. Appl Catal Gen 2014;482:163–70. https://doi.org/10.1016/j.apcata.2014.05.037.
[55] Tavasoli A, Barati M, Karimi A. Conversion of sugarcane bagasse to gaseous and liquid fuels in near-critical water media using K2O promoted Cu/γ-Al2O3-MgO nanocatalysts. Biomass Bioenergy 2015;80:63–72. https://doi.org/10.1016/j.biombioe.2015.04.031.
[56] Alipour Z, Meshkani F, Rezaei M. Effect of K2O on the catalytic performance of Ni catalysts supported on nanocrystalline Al 2O3 in CO2 reforming of methane. Iran J Hydrog Fuel Cell 2015;4:215–26.
[57] Yang M, Lingjun Z, Xiaonan Z, Prasert R, Shurong W. CO2 methanation over nickel-based catalysts supported on MCM-41 with in situ doping of zirconium. J CO2 Util 2020;42:101304. https://doi.org/10.1016/j.jcou.2020.101304.
[58] Liu X, Sun L, Deng WQ. Theoretical investigation of CO2 adsorption and dissociation on low index surfaces of transition metals. J Phys Chem C 2018;122:8306–14. https://doi.org/10.1021/acs.jpcc.7b12660.
[61] Nabgan W, Tuan Abdullah TA, Mat R, Nabgan B, Gambo Y, Triwahyono S. Influence of Ni to Co ratio supported on ZrO2 catalysts in phenol steam reforming for hydrogen production. Int J Hydrogen Energy 2016;41:22922–31. https://doi.org/10.1016/j.ijhydene.2016.10.055.
[62] Turap Y, Wang I, Fu T, Wu Y, Wang Y, Wang W. Co–Ni alloy supported on CeO2 as a bimetallic catalyst for dry reforming

of methane. Int J Hydrogen Energy 2020;45:6538–48. https://doi.org/10.1016/j.ijhydene.2019.12.223.
[63] Ochoa A, Bilbao J, Gayubo AG, Castaño P. Coke formation and deactivation during catalytic reforming of biomass and waste pyrolysis products: a review. Renew Sustain Energy Rev 2020;119:109600. https://doi.org/10.1016/j.rser.2019.109600.
[64] Navarro RM, Guil-Lopez R, Ismail AA, Al-Sayari SA, Fierro JLG. Ni- and PtNi-catalysts supported on Al2O3 for acetone steam reforming: effect of the modification of support with Ce, La and Mg. Catal Today 2015;242:60–70. https://doi.org/10.1016/j.cattod.2014.07.036.
[65] Zhang Z, Hu X, Li J, Gao G, Dong D, Westerhof R, et al. Steam reforming of acetic acid over Ni/Al2O3 catalysts: correlation of nickel loading with properties and catalytic behaviors of the catalysts. Fuel 2018;217:389–403. https://doi.org/10.1016/j.fuel.2017.12.114.
[66] Wang Z, Wang C, Chen S, Liu Y. Co-Ni bimetal catalyst supported on perovskite-type oxide for steam reforming of ethanol to produce hydrogen. Int J Hydrogen Energy 2014;39:5644–52. https://doi.org/10.1016/j.ijhydene.2014.01.151.
[67] Megía PJ, Cortese M, Ruocco C, Vizcaíno AJ, Calles JA, Carrero A, et al. Catalytic behavior of co-based catalysts in the kinetic study of acetic acid steam reforming. Ind Eng Chem Res 2020;59:19531–8. https://doi.org/10.1021/acs.iecr.0c03599.
[68] Kumar A, Sinha ASK. Hydrogen production from acetic acid steam reforming over nickel-based catalyst synthesized via MOF process. Int J Hydrogen Energy 2020;45:24397–411. https://doi.org/10.1016/j.ijhydene.2020.06.040.
[69] Fu M, Qi W, Xu Q, Zhang S, Yan Y. Hydrogen production from bio-oil model compounds dry (CO2) reforming over Ni/Al2O3 catalyst. Int J Hydrogen Energy 2016;41:1494–501. https://doi.org/10.1016/j.ijhydene.2015.11.104.
[70] Vizcaíno AJ, Carrero A, Calles JA. Hydrogen production by ethanol steam reforming over Cu-Ni supported catalysts. Int J Hydrogen Energy 2007;32:1450–61. https://doi.org/10.1016/j.ijhydene.2006.10.024.
[71] Afolabi ATF, Kechagiopoulos PN, Liu Y, Li CZ. Kinetic features of ethanol steam reforming and decomposition using a biochar-supported Ni catalyst. Fuel Process Technol 2021;212:106622. https://doi.org/10.1016/j.fuproc.2020.106622.
[72] Comas J, Marino F, Laborde M, Amadeo N. Bio-ethanol steam reforming on Ni/Al2O3 catalyst. Chem Eng J 2004;98:61–8. https://doi.org/10.1016/S1385-8947(03)00186-4.
[73] Lahijani P, Zainal ZA, Mohammadi M, Mohamed AR. Conversion of the greenhouse gas CO2 to the fuel gas CO via the Boudouard reaction: a review. Renew Sustain Energy Rev 2015;41:615–32. https://doi.org/10.1016/j.rser.2014.08.034.
[74] Ledesma EB, Campos C, Cranmer DJ, Foytik BL, Ton MN, Dixon EA, et al. Vapor-phase cracking of eugenol: distribution of tar products as functions of temperature and residence time. Energy Fuels 2013;27:868–78. https://doi.org/10.1021/ef3018332.
[75] Lu P, Qian X, Huang Q, Chi Y, Yan J. Catalytic cracking of toluene as a tar model compound using sewage-sludge-derived char. Energy Fuels 2016;30:8327–34. https://doi.org/10.1021/acs.energyfuels.6b01832.
[76] Li J, Mei X, Zhang L, Yu Z, Liu Q, Wei T, et al. A comparative study of catalytic behaviors of Mn, Fe, Co, Ni, Cu and Zn–Based catalysts in steam reforming of methanol, acetic acid and acetone. Int J Hydrogen Energy 2020;45:3815–32. https://doi.org/10.1016/j.ijhydene.2019.03.269.
[77] Hu X, Dong D, Shao X, Zhang L, Lu G. Steam reforming of acetic acid over cobalt catalysts: effects of Zr, Mg and K addition. Int J Hydrogen Energy 2017;42:4793–803. https://doi.org/10.1016/j.ijhydene.2016.12.033.
[78] Wu Y, Pang Y, Chen Y, Zhai M, Zheng M. Study on the steam gasification reaction of biomass char under the synergistic effect of Ca-Fe: analysis of kinetic characteristics. Int J Energy Res 2021:1–15. https://doi.org/10.1002/er.6366.
[79] Wanke SE, Flynn PC. The sintering of supported metal catalysts. Catal Rev 1975;12:93–135. https://doi.org/10.1080/01614947508067523.
[80] Kumar A, Sinha ASK. Hydrogen production from acetic acid steam reforming over nickel-based catalyst synthesized via MOF process. Int J Hydrogen Energy 2020;45:24397–411. https://doi.org/10.1016/j.ijhydene.2020.06.040.
[81] Mahamulkar S, Yin K, Agrawal PK, Davis RJ, Jones CW, Malek A, et al. Formation and oxidation/gasification of carbonaceous deposits: a review. Ind Eng Chem Res 2016;55:9760–818. https://doi.org/10.1021/acs.iecr.6b02220.
[82] Santamaria L, Artetxe M, Lopez G, Cortazar M, Amutio M, Bilbao J, et al. Effect of CeO2 and MgO promoters on the performance of a Ni/Al2O3 catalyst in the steam reforming of biomass pyrolysis volatiles. Fuel Process Technol 2020;198:106223. https://doi.org/10.1016/j.fuproc.2019.106223.
[83] Hervy M, Weiss-Hortala E, Pham Minh D, Dib H, Villot A, Gérente C, et al. Reactivity and deactivation mechanisms of pyrolysis chars from bio-waste during catalytic cracking of tar. Appl Energy 2019;237:487–99. https://doi.org/10.1016/j.apenergy.2019.01.021.
[84] Chen J, Wang M, Wang S, Li X. Hydrogen production via steam reforming of acetic acid over biochar-supported nickel catalysts. Int J Hydrogen Energy 2018;43:18160–8. https://doi.org/10.1016/j.ijhydene.2018.08.048.
[85] Da Silva ALM, Den Breejen JP, Mattos LV, Bitter JH, De Jong KP, Noronha FB. Cobalt particle size effects on catalytic performance for ethanol steam reforming - smaller is better. J Catal 2014;318:67–74. https://doi.org/10.1016/j.jcat.2014.07.020.
[86] Chang JR, Chang SL, Lin TB. γ-Alumina-supported Pt catalysts for aromatics reduction: a structural investigation of sulfur poisoning catalyst deactivation. J Catal 1997;169:338–46. https://doi.org/10.1006/jcat.1997.1709.
[87] Marquevich M, Czernik S, Chornet E, Montané D. Hydrogen from biomass: steam reforming of model compounds of fast-pyrolysis oil. Energy Fuels 1999;13:1160–6. https://doi.org/10.1021/ef990034w.
[88] Belin T, Epron F. Characterization methods of carbon nanotubes: a review. Mater Sci Eng B 2005;119:105–18. https://doi.org/10.1016/j.mseb.2005.02.046.
[89] Liu W, Chai S, Mohamed AR, Hashim U. Synthesis and characterization of graphene and carbon nanotubes: a review on the past and recent developments. J Ind Eng Chem 2014;20:1171–85. https://doi.org/10.1016/j.jiec.2013.08.028.
[90] Hu X, Wang Y, Mourant D, Gunawan R, Lievens C, Chaiwat W, et al. Polymerization on heating up of bio-oil: a model compound study. AIChE J 2013;59:888–900. https://doi.org/10.1002/aic.13857.
[91] Zhang L, Yu Z, Li J, Zhang S, Hu S, Xiang J, et al. Steam reforming of typical small organics derived from bio-oil: correlation of their reaction behaviors with molecular structures. Fuel 2020;259:116214. https://doi.org/10.1016/j.fuel.2019.116214.